genotype comparison	total # of windows in comparison	# of windows advanced	# of windows delayed
WT mitotic follicle vs. WT wing disc	13391	1951 (earlier in follicle)	1943 (earlier in wing)
WT endo follilcle vs. WT mitotic follicle	13391	0	0
Rif1^{-} wing disc vs. WT wing disc	13391	552	527
Rif1^{-} mitotic follicle vs. WT mitotic follicle	13391	1095	672
Rif1$^{-/+}$ mitotic follicle vs. WT mitotic follicle	13391	478	212
Rif1^{-} endo follicle vs. WT endo follicle	13391	960	1024
Rif1^{PP1} wing disc vs. WT wing disc	13391	1726	666
Rif1^{PP1} mitotic follicle vs. WT mitotic follicle	13391	968	520

Table S1. Quantification of differential RT at 100kb windows using a 10kb slide across the major chromosome scaffolds.

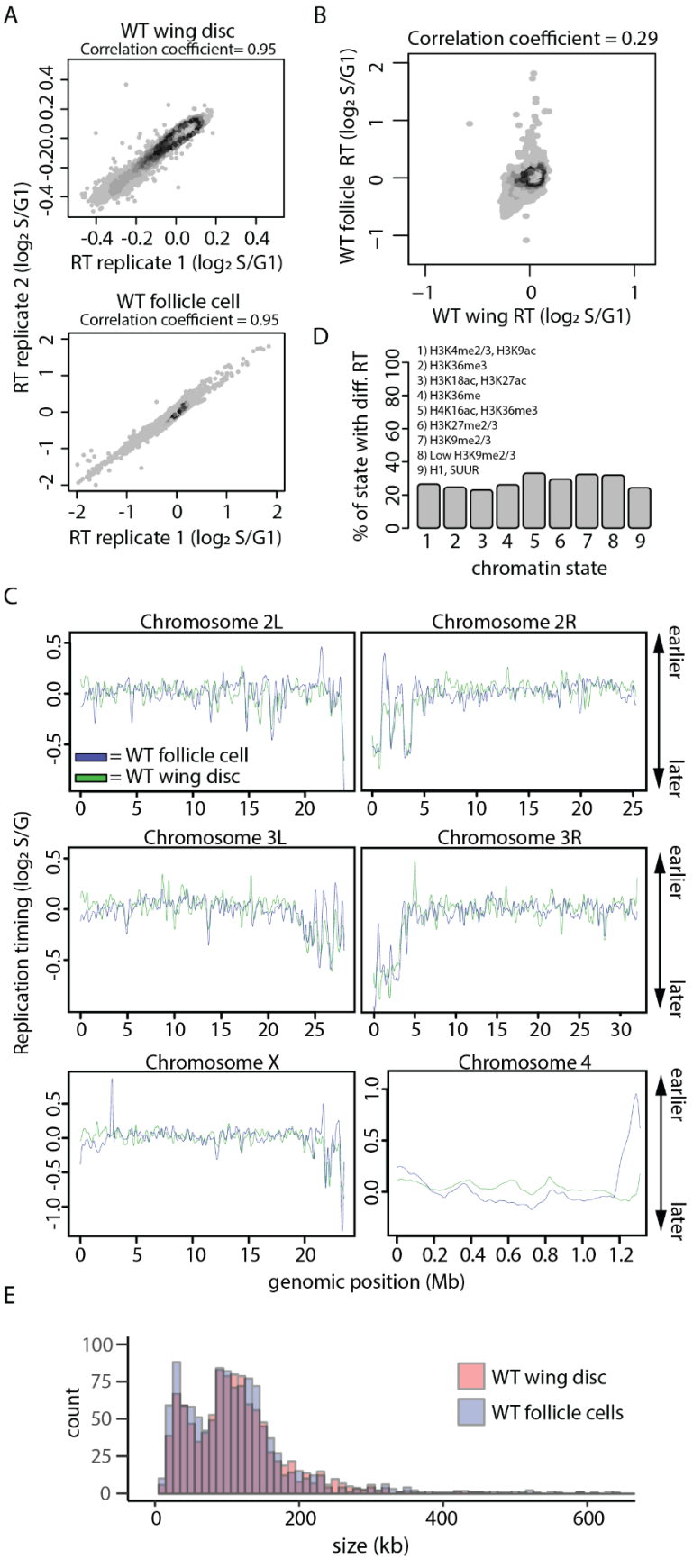
A
WT wing disc
Correlation coefficient= 0.95
RT replicate 2 (log2 S/G1)
RT replicate 1 (log2 S/G1)
WT follicle cell
Correlation coefficient = 0.95
RT replicate 2 (log2 S/G1)
RT replicate 1 (log2 S/G1)
B
Correlation coefficient = 0.29
WT follicle RT (log2 S/G1)
WT wing RT (log2 S/G1)
D
1) H3K4me2/3, H3K9ac
2) H3K36me3
3) H3K18ac, H3K27ac
4) H3K36me
5) H4K16ac, H3K36me3
6) H3K27me2/3
7) H3K9me2/3
8) Low H3K9me2/3
9) H1, SUUR
% of state with diff. RT
chromatin state
C
Chromosome 2L
Chromosome 2R
= WT follicle cell
= WT wing disc
earlier
later
Chromosome 3L
Chromosome 3R
Chromosome X
Chromosome 4
Replication timing (log2 S/G)
genomic position (Mb)
E
count
WT wing disc
WT follicle cells
size (kb)

Figure S1. Characterization of RT in wildtype wing discs and follicle cells. A) Heatscatter plot comparing wildtype wing disc S/G1 (log_2) replicate replication timing values (top) and wildtype follicle cell S/G1 (log_2) replicate replication timing values (bottom). **B)** Heatscatter plot of wildtype wing disc and wildtype follicle cell S/G1 (log_2) ratios at 100kb windows using a 10kb slide across all chromosome arms (pericentric sequences were removed from the genome). **C)** LOESS regression line showing average S/G1 (log_2) replication timing values for wildtype wings discs (green) and wildtype follicle cells (blue) at 100kb windows using a 10kb slide across the major chromosome scaffolds. **D)** All 10kb windows of differential RT between wildtype follicle cells and wild type wing discs were assigned to the nine chromatin states previously defined in *Drosophila* (Kharchenko et al. 2011). Shown are the percentage of each chromatin state with differential RT. **E)** Histogram of replication domain sizes in wildtype follicle cells and wildtype wing discs.

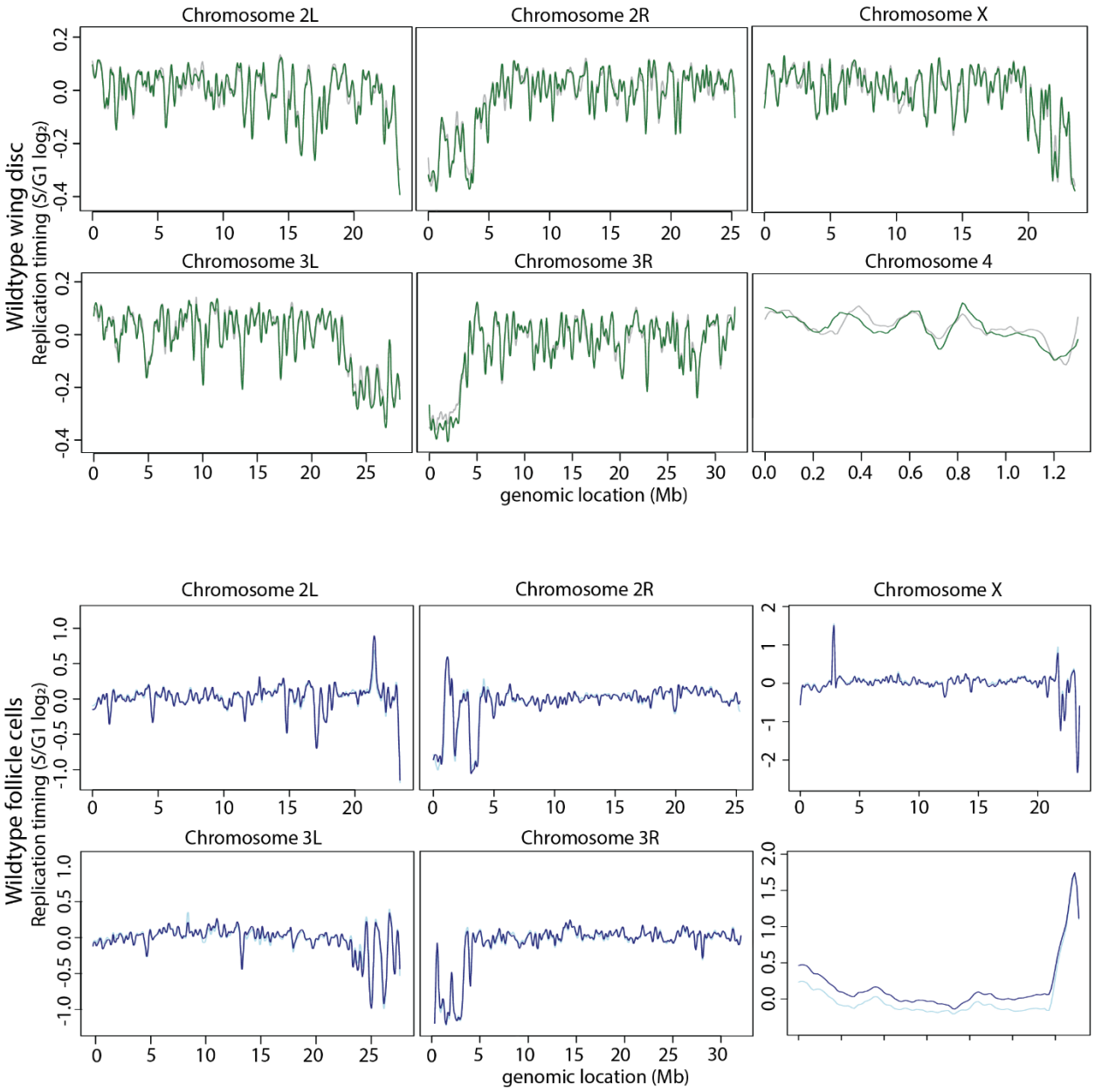

Figure S2. Replication timing profiling in *Drosophila* is highly reproducible. Quantile normalized S/G1 (log_2) replication timing values for each replicate for the indicated genotypes were plotted versus genomic coordinate for all major chromosome scaffolds. Each replicate for wild type wing disc and wild type follicle cells is shown in a different color (green and grey, wing disc; navy blue and light blue, follicle cells).

A

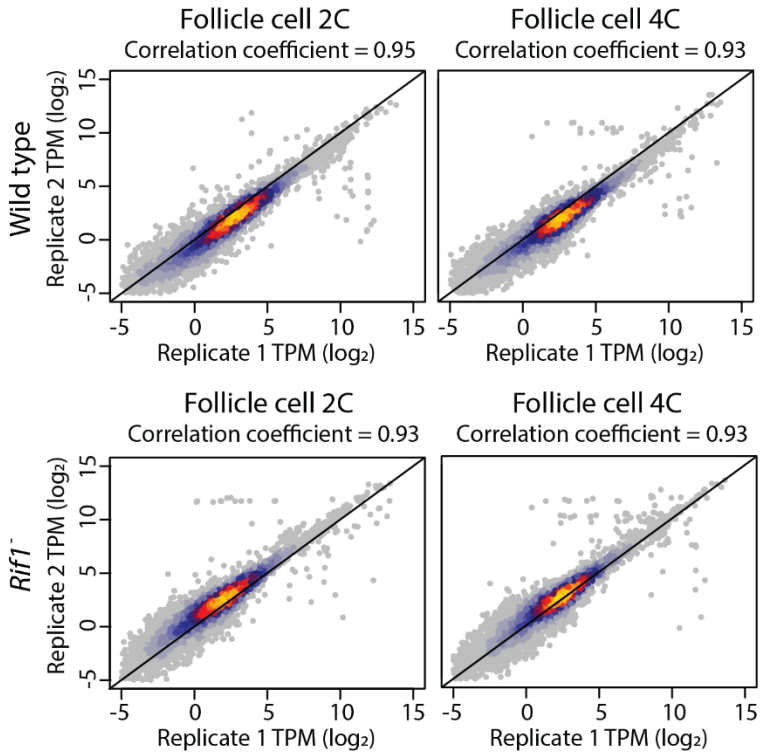
Follicle cell 2C
Correlation coefficient = 0.95
Follicle cell 4C
Correlation coefficient = 0.93
Wild type
Replicate 2 TPM (log2)
Replicate 1 TPM (log2)
Follicle cell 2C
Correlation coefficient = 0.93
Follicle cell 4C
Correlation coefficient = 0.93
Rif1-
Replicate 2 TPM (log2)
Replicate 1 TPM (log2)

B

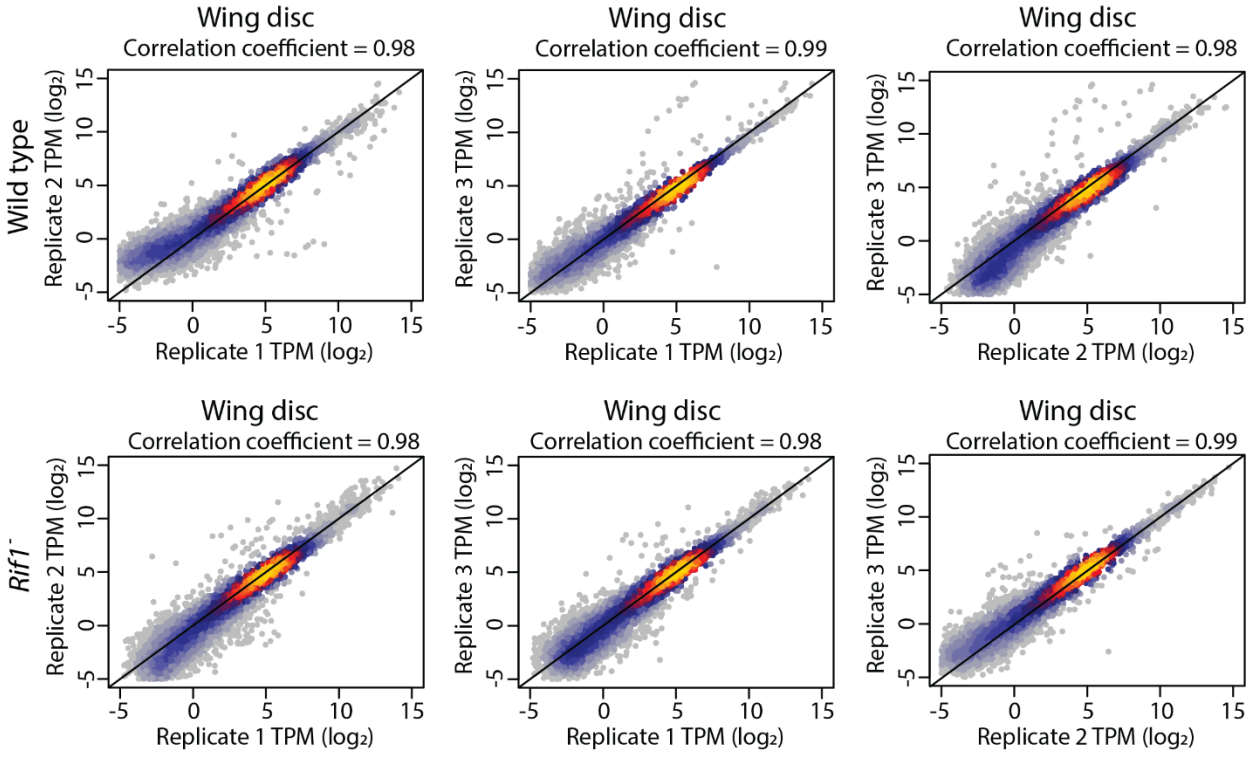
Wing disc
Correlation coefficient = 0.98
Wing disc
Correlation coefficient = 0.99
Wing disc
Correlation coefficient = 0.98
Wild type
Replicate 2 TPM (log2)
Replicate 3 TPM (log2)
Replicate 1 TPM (log2)
Replicate 2 TPM (log2)
Wing disc
Correlation coefficient = 0.98
Wing disc
Correlation coefficient = 0.98
Wing disc
Correlation coefficient = 0.99
Rif1-
Replicate 2 TPM (log2)
Replicate 3 TPM (log2)
Replicate 1 TPM (log2)
Replicate 2 TPM (log2)

Figure S3. Replicate correlations of RNA-seq data. A) Heatscatter plot comparing wildtype follicle cell RNA-seq transcript per million (TPM) values (log_2; top) and *Rif1*$^-$ follicle cell RNA-seq transcript per million (TPM) values (log_2; bottom). **B)** Heatscatter plot comparing wildtype wing disc RNA-seq transcript per million (TPM) values (log_2; top) and *Rif1*$^-$ wing disc RNA-seq transcript per million (TPM) values (log_2; bottom).

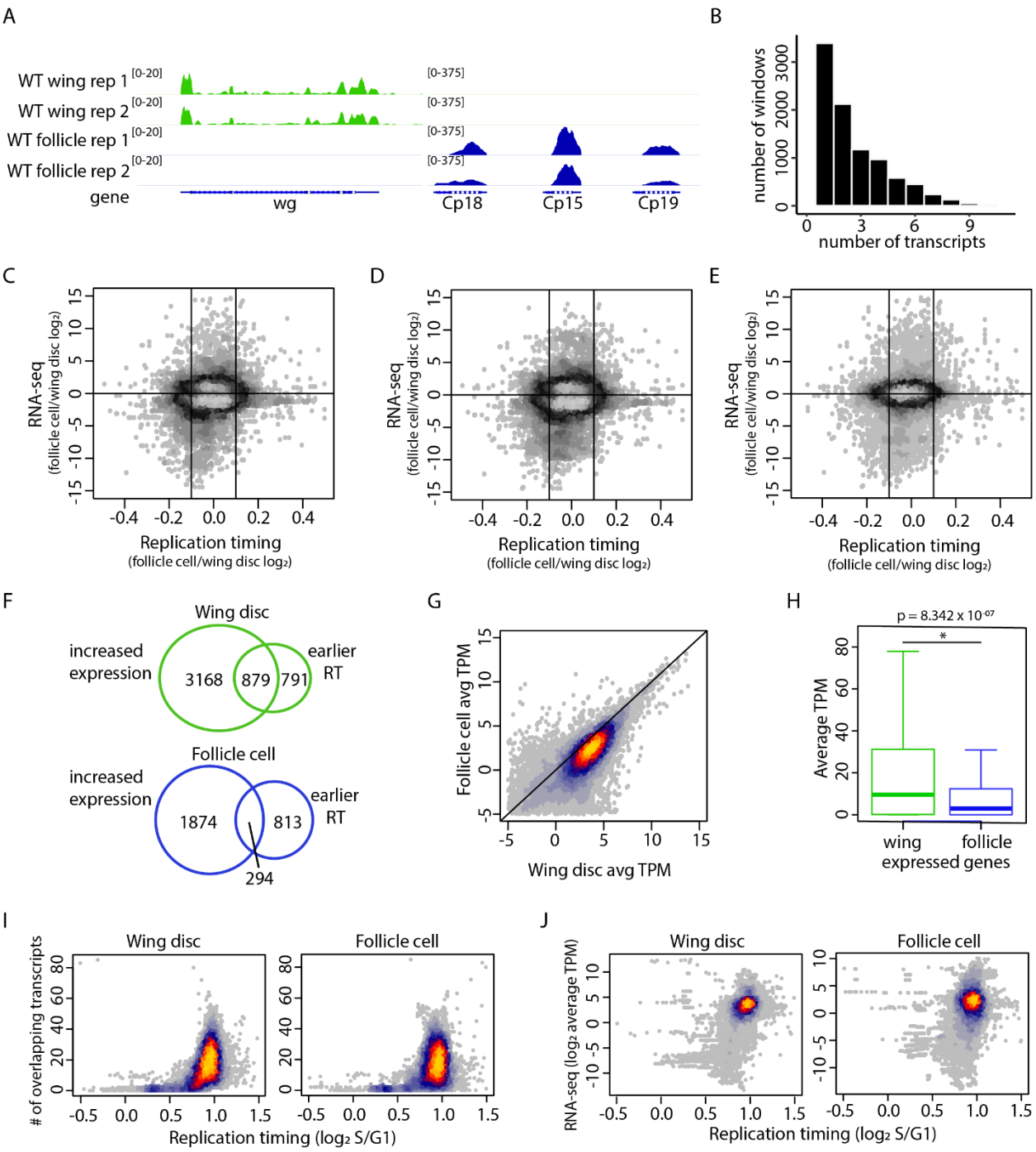

Figure S4. Transcriptional change does not drive differential RT between lineages. A) Genome browser shot of representative lineage-specific genes, wingless (wg) and chorion proteins 18, 15, and 19 (Cp18, Cp15, and Cp19). RNA-seq signal is shown for two replicates of wildtype wing discs (green) and wild type follicle cells (blue). **B)** Histogram of the number of transcripts

overlapping each 10kb window. Only windows containing at least one transcript are shown. **C)** Heatscatter plot of the wildtype follicle cell/wildtype wing disc RT values (S/G1 (log_2)) versus the wildtype follicle cell/wildtype wing disc ratio of the transcriptional change of the most confident transcript (lowest p value) at each window across the major chromosome scaffolds. Only windows containing at least one transcript are shown. **D)** Heatscatter plot of the wildtype follicle cell/wildtype wing disc RT values (S/G1 (log_2)) versus the wildtype follicle cell/wildtype wing disc ratio of the transcriptional change of the transcript with the greatest differential expression (absolute maximum log_2 fold-change) at each window across the major chromosome scaffolds. Only windows containing at least one transcript are shown. **E)** Heatscatter plot of the wildtype follicle cell/wildtype wing disc RT values (S/G1 (log_2)) versus the wildtype follicle cell/wildtype wing disc ratio of the transcriptional change of at all genes. **F)** Venn diagrams comparing 10kb windows of significantly increased gene expression in wing discs ($p < 0.01$, log_2 fold change < 0; edgeR) to significantly earlier replication in wing discs ($p < 0.05$, log_2 fold change < -0.1; limma) (top; green) and comparing windows of significantly increased gene expression in follicle cells ($p < 0.01$, log_2 fold change > 0; edgeR) to significantly earlier replication in follicle cells ($p < 0.05$, log_2 fold change > 0.1; limma) (bottom; blue). **G)** Heatscatter plot comparing wildtype wing disc RNA-seq signal and wildtype follicle cell RNA-seq signal. **H)** Quantification of RNA-seq signal. **I)** Heatscatter plot of wild type wing disc (top) and wild type follicle cell (bottom) S/G1 (log_2) replication timing values versus the number of transcripts within 10kb windows across the major chromosome scaffolds. **J)** Heatscatter plot of wild type wing disc (top) and wild type follicle cell (bottom) S/G1 (log_2) replication timing values versus the average transcriptional activity within 10kb windows across the major chromosome scaffolds.

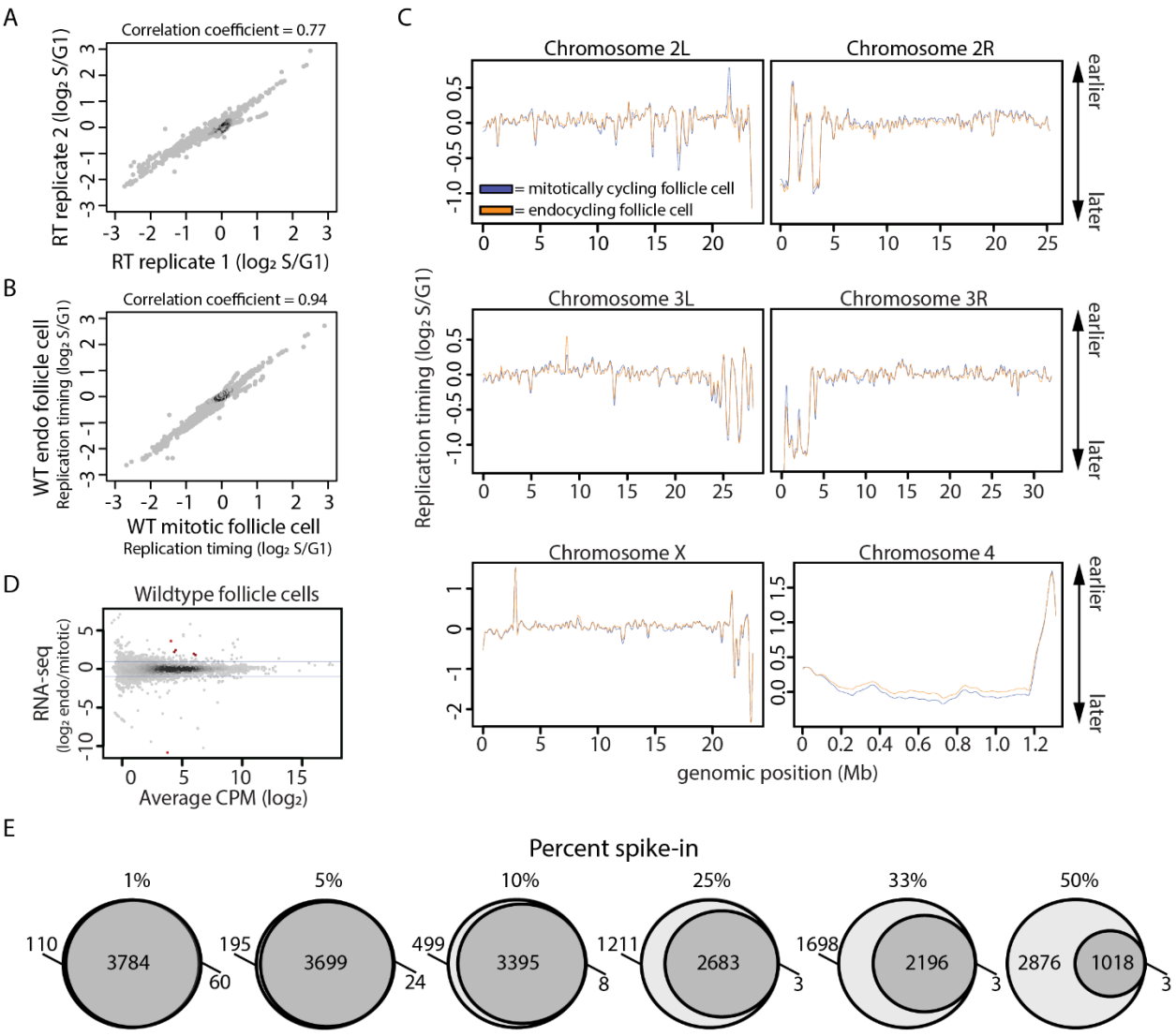

Figure S5. Characterization of RT between wildtype mitotically cycling and endocycling follicle cells. A) Heatscatter plot comparing wildtype endocycling follicle cell S/G1 (log_2) replicate replication timing values. **B)** Heatscatter plot comparing wildtype mitotically cycling follicle cell and endocycling follicle cells S/G1 (log_2) ratios at all 100kb windows using a 10kb slide across all major chromosome scaffolds. **C)** LOESS regression line showing average S/G1 (log_2) replication timing values for wildtype mitotically cycling follicle cells (blue) and wildtype endocycling follicle cells (orange) at 100kb windows using a 10kb slide across the major chromosome scaffolds. **D)** Heatscatter plot of the wildtype endocycling follicle cell/wildtype mitotically cycling

follicle cell ratio of total RNA-seq signal. Statistically different transcripts between wildtype follicle cells and wildtype wing discs are indicated in red ($p < 0.01$; edgeR). Blue lines indicate a $\log_2$ fold change of 1 and -1. **E)** Venn diagram comparisons of significant RT changes identified between *in* silico-generated spike-in datasets (Materials and methods) and wildtype wing imaginal discs (dark grey) versus significant RT changes identified between wildtype follicle cells and wildtype wing imaginal discs (light grey; $p < 0.01$, absolute $\log_2$ fold change > 0.1; limma).

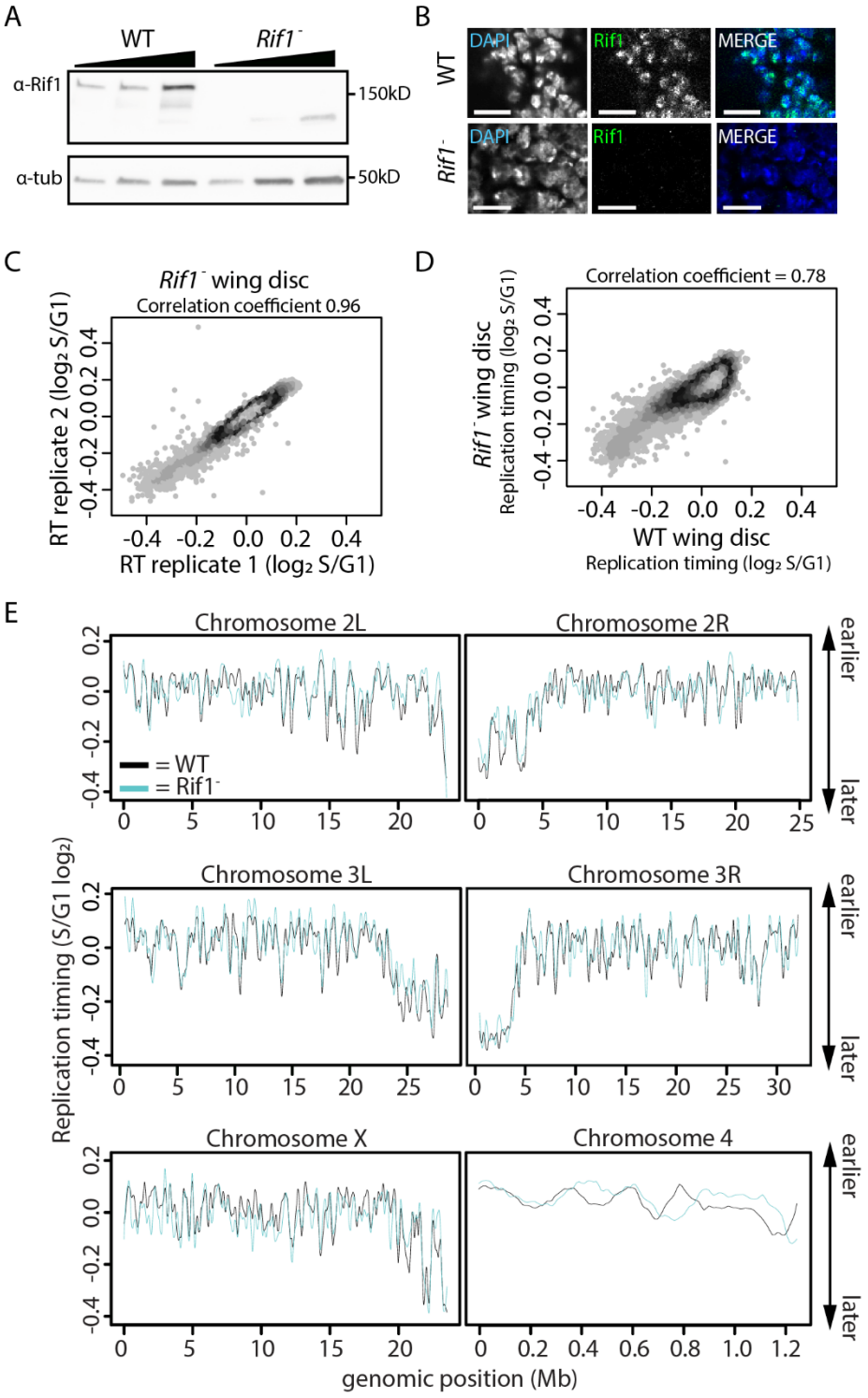

Figure S6. Characterization of RT in *Rif1*⁻ wing imaginal discs. A) Western blot analysis of protein isolated from 10, 20, and 40 wildtype and *Rif1*⁻ wing discs (left to right). **B)** Wild type and *Rif1*⁻ wing imaginal disc cells stained with DAPI (blue) and anti-Rif1 (green) antibodies.

Bar, 10 μm. **C)** Heatscatter plot comparing *Rif1*$^{-}$ wing disc S/G1 (log_2) replicate replication timing values. **D)** Heatscatter plot comparing wildtype and *Rif1*$^{-}$ wing disc S/G1 (log_2) ratios at 100kb windows using a 10kb slide across all major chromosome scaffolds. **E)** LOESS regression line showing average S/G1 (log_2) replication timing values for wildtype wing discs (black) and *Rif1*$^{-}$ wing discs (cyan) at 100kb windows using a 10kb slide across the major chromosome scaffolds.

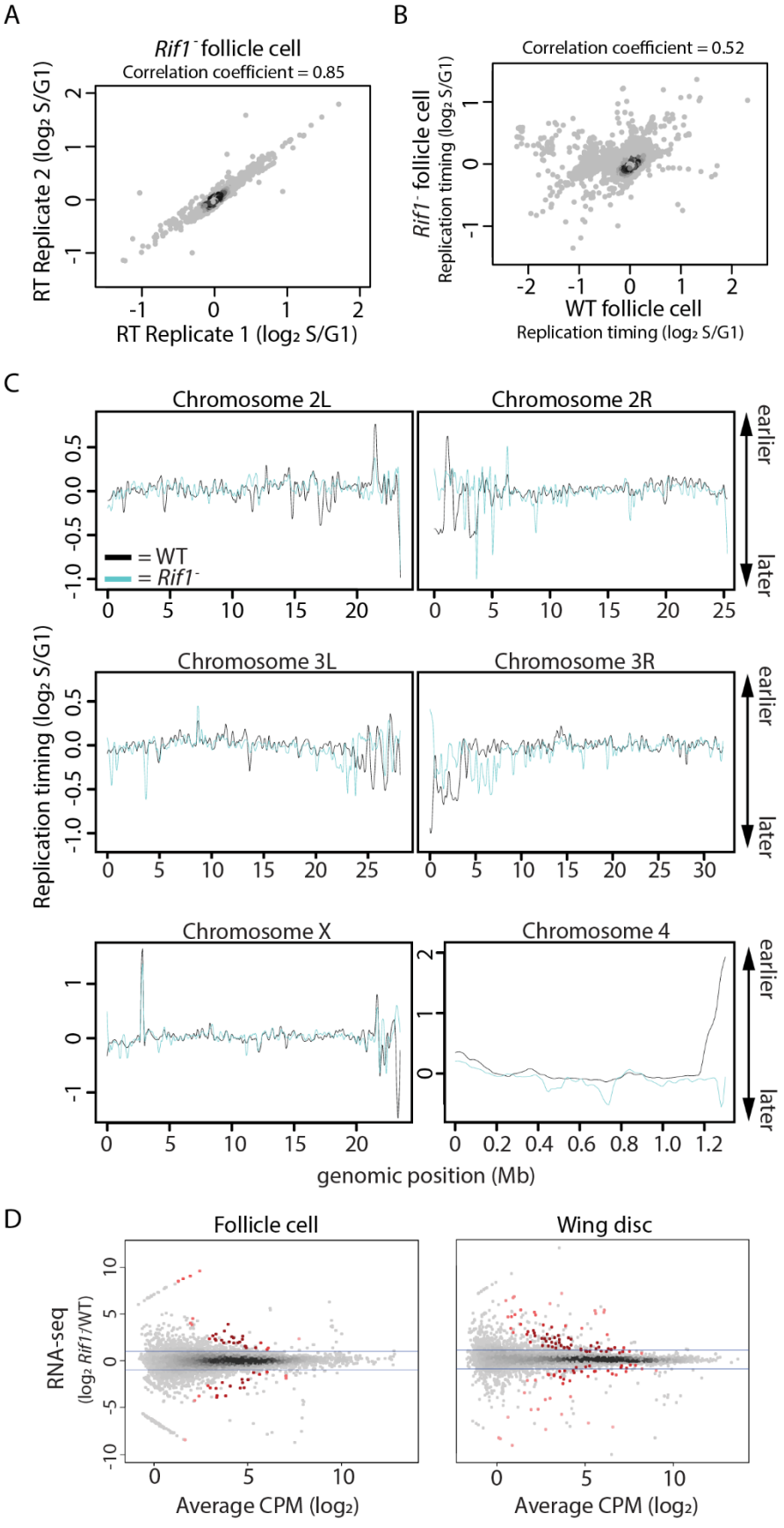
A
Rif1- follicle cell
Correlation coefficient = 0.85
RT Replicate 2 (log2 S/G1)
RT Replicate 1 (log2 S/G1)
B
Correlation coefficient = 0.52
Rif1- follicle cell
Replication timing (log2 S/G1)
WT follicle cell
Replication timing (log2 S/G1)
C
Chromosome 2L
Chromosome 2R
= WT
= Rif1-
earlier
later
Chromosome 3L
Chromosome 3R
Replication timing (log2 S/G1)
Chromosome X
Chromosome 4
genomic position (Mb)
D
Follicle cell
Wing disc
RNA-seq
(log2 Rif1/WT)
Average CPM (log2)

Figure S7. Characterization of RT in *Rif1*$^{-}$ mitotically cycling follicle cells. A) Heatscatter plot comparing *Rif1*$^{-}$ mitotically cycling follicle cell S/G1 (log_2) replicate replication timing values. **B)** Heatscatter plot comparing wildtype and *Rif1*$^{-}$ mitotically cycling follicle cell S/G1 (log_2) ratios at 100kb windows using a 10kb slide across all major chromosome scaffolds. C**)** LOESS regression line showing average S/G1 (log_2) replication timing values for wildtype mitotically cycling follicle cells (black) and *Rif1*$^{-}$ mitotically cycling follicle cells (cyan) at 100kb windows using a 10kb slide across the major chromosome scaffolds. **D)** Heatscatter plot of the *Rif1*$^{-}$/control ratio of total RNA-seq signal in follicle cells (top) and wing discs (bottom). Statistically different transcripts are indicated in red ($p < 0.01$; edgeR). Blue lines indicate a log_2 fold change of 1 and -1.

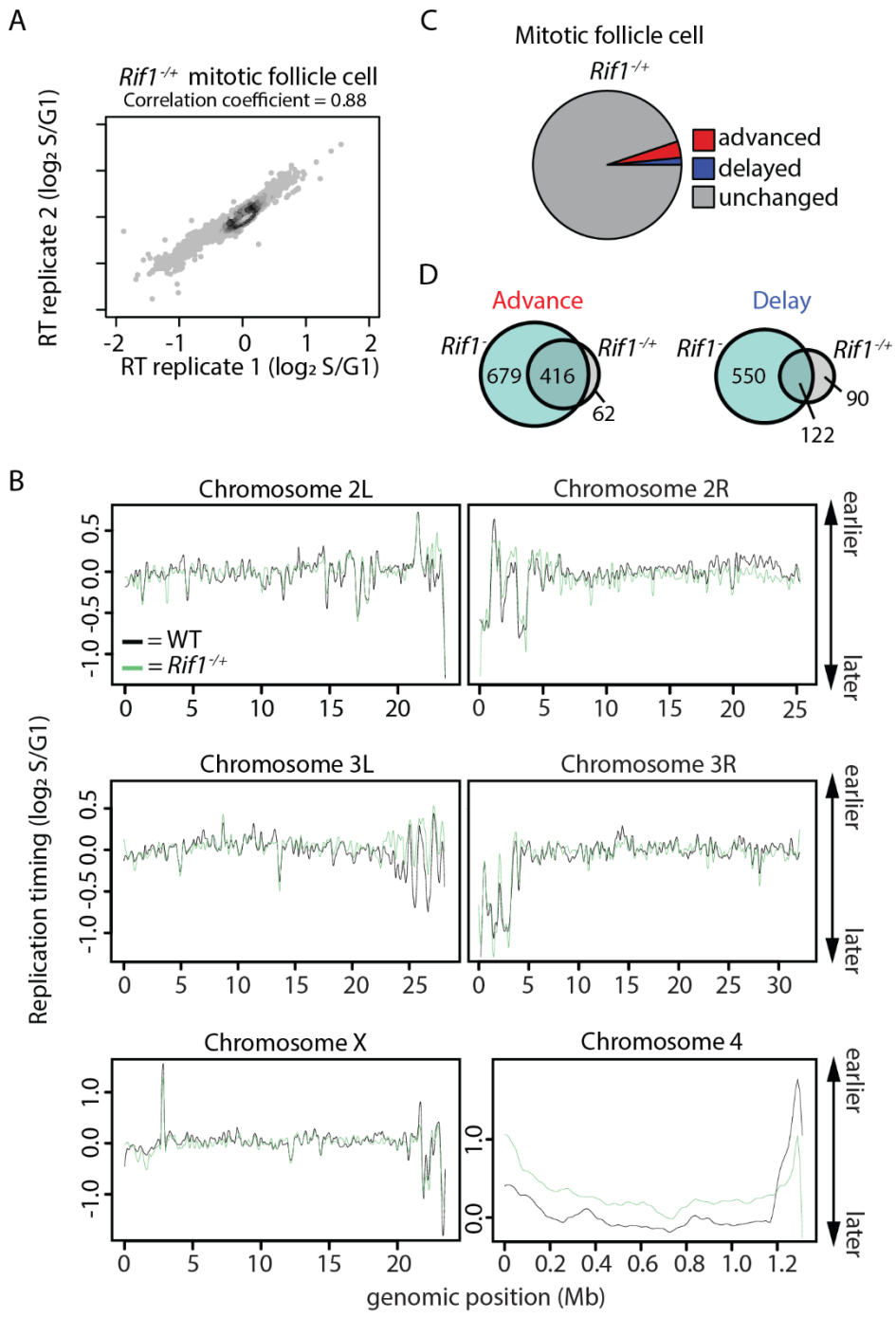

Figure S8. Characterization of RT in *Rif1*$^{-/+}$ mitotic follicle cells. A) Heatscatter plot comparing *Rif1*$^{-/+}$ mitotic follicle cell S/G1 (log_2) replicate replication timing values. **B)** LOESS regression line showing average S/G1 (log_2) replication timing values for wildtype mitotic follicle cells (black) and *Rif1*$^{-/+}$ mitotic follicle cells (light green) at 100kb windows using a 10kb slide across

the major chromosome scaffolds. **C)** Pie chart of all 100kb windows of significantly advanced (red), delayed (blue), and unchanged RT (grey) in *Rif1*$^{-/+}$ mitotic follicle cells across the major chromosome scaffolds. **D)** Venn diagrams comparing significantly advanced (left) and delayed (right) 100kb windows identified in *Rif1*$^{-}$ and *Rif1*$^{-/+}$ follicle cells ($p<0.01$ and absolute $\log_2$ fold change > 0.1; limma).

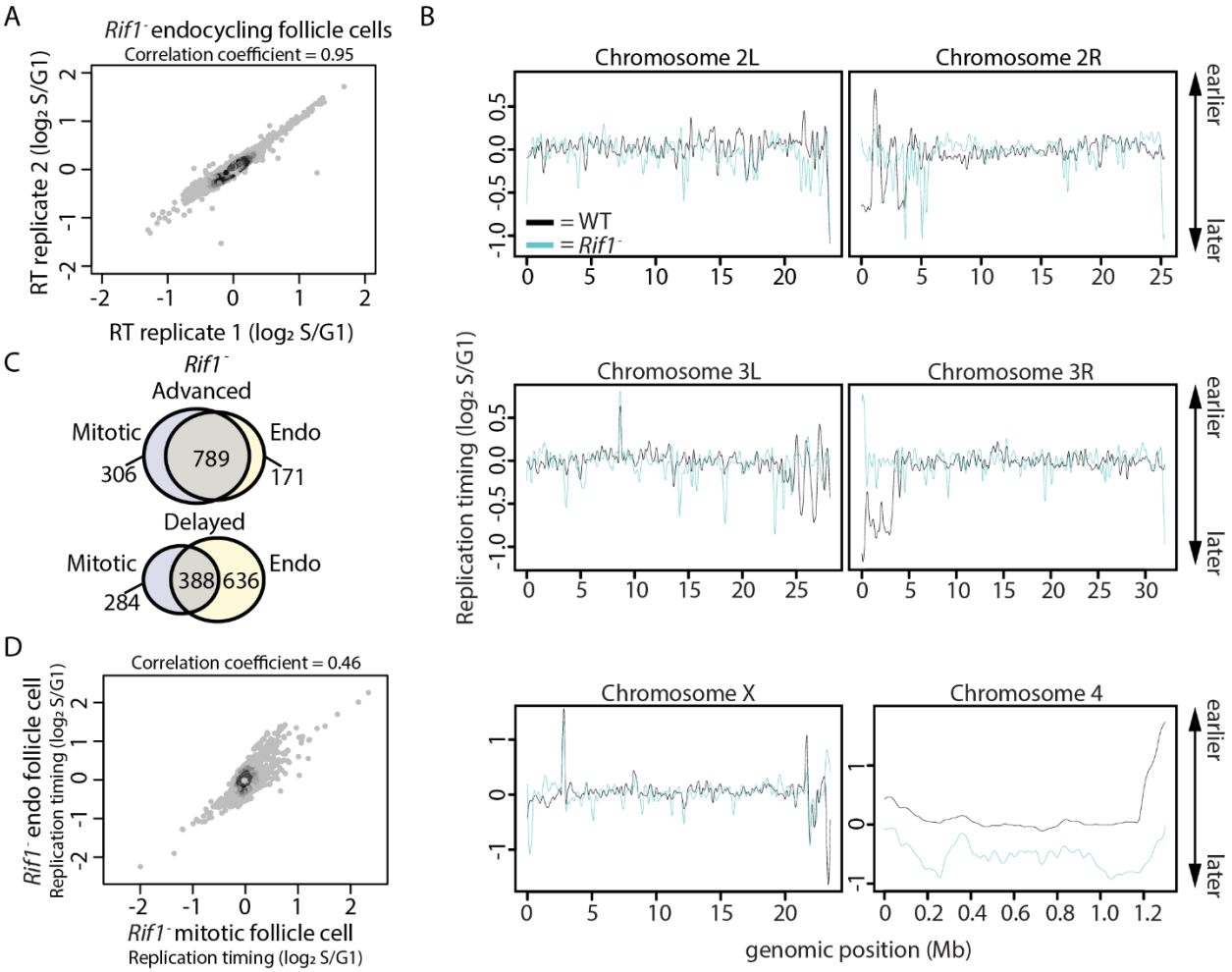

Figure S9. Characterization of RT in *Rif1*⁻ endocycling cycling follicle cells. A) Heatscatter plot comparing *Rif1*⁻ endocycling follicle cell S/G1 (log_2) replicate replication timing values. **B)** LOESS regression line showing average S/G1 (log_2) replication timing values for wildtype mitotically cycling follicle cells (black) and *Rif1*⁻ mitotically cycling follicle cells (cyan) at 100kb windows using a 10kb slide across the major chromosome scaffolds. **C)** Venn diagrams comparing significant advanced (top) and significantly delayed (bottom) RT changes identified in *Rif1*⁻ mitotically cycling follicle cells (left) and *Rif1*⁻ endocycling follicle cells (right). **D)** Heatscatter plot comparing *Rif1*⁻ mitotically cycling and endocycling follicle cell S/G1 (log_2) ratios at 100kb windows using a 10kb slide across all major chromosome scaffolds.

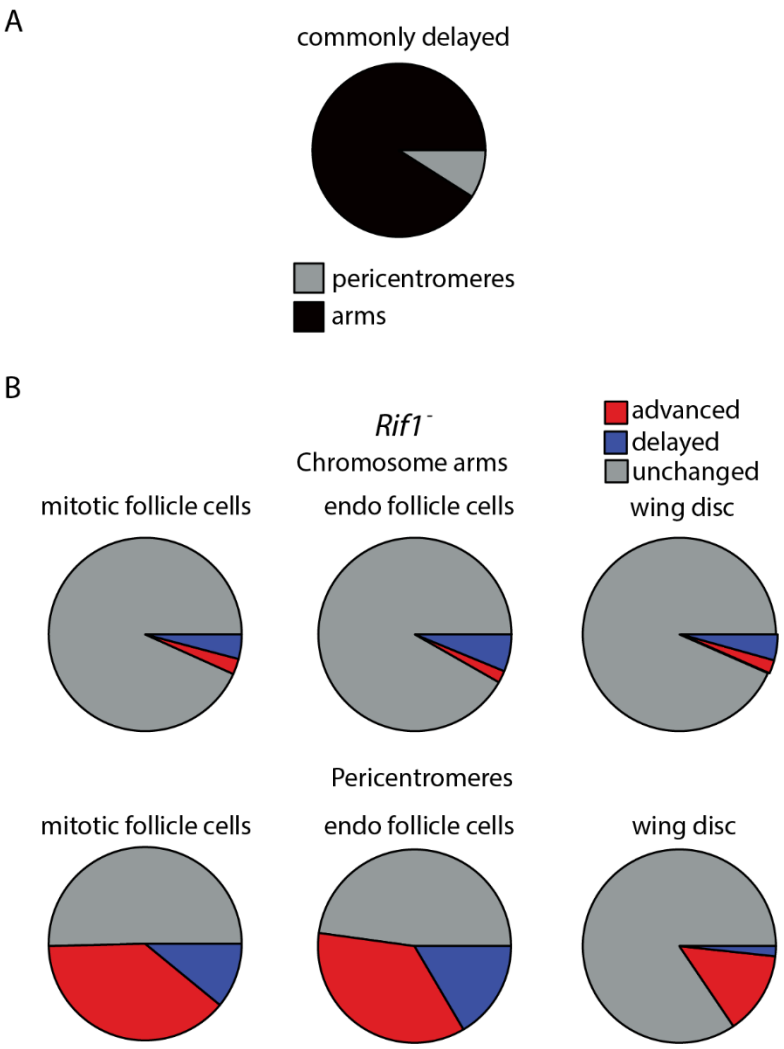

Figure S10. Characterization of Rif1-dependent RT control in follicle cells and wing discs. **A)** Pie chart of all 100kb windows of commonly delayed RT between *Rif1*- wing discs and follicle cells. Windows located within pericentromeres are in grey and windows located within chromosome arms are in black. **B)** Pie charts of all 100kb windows with advanced (red), delayed (blue), and unchanged (grey) RT in *Rif1*$^{-}$ mitotically cycling follicle cells, endocycling follicle cells, and wing discs separated by chromosome arms (top) and pericentromeres (bottom).

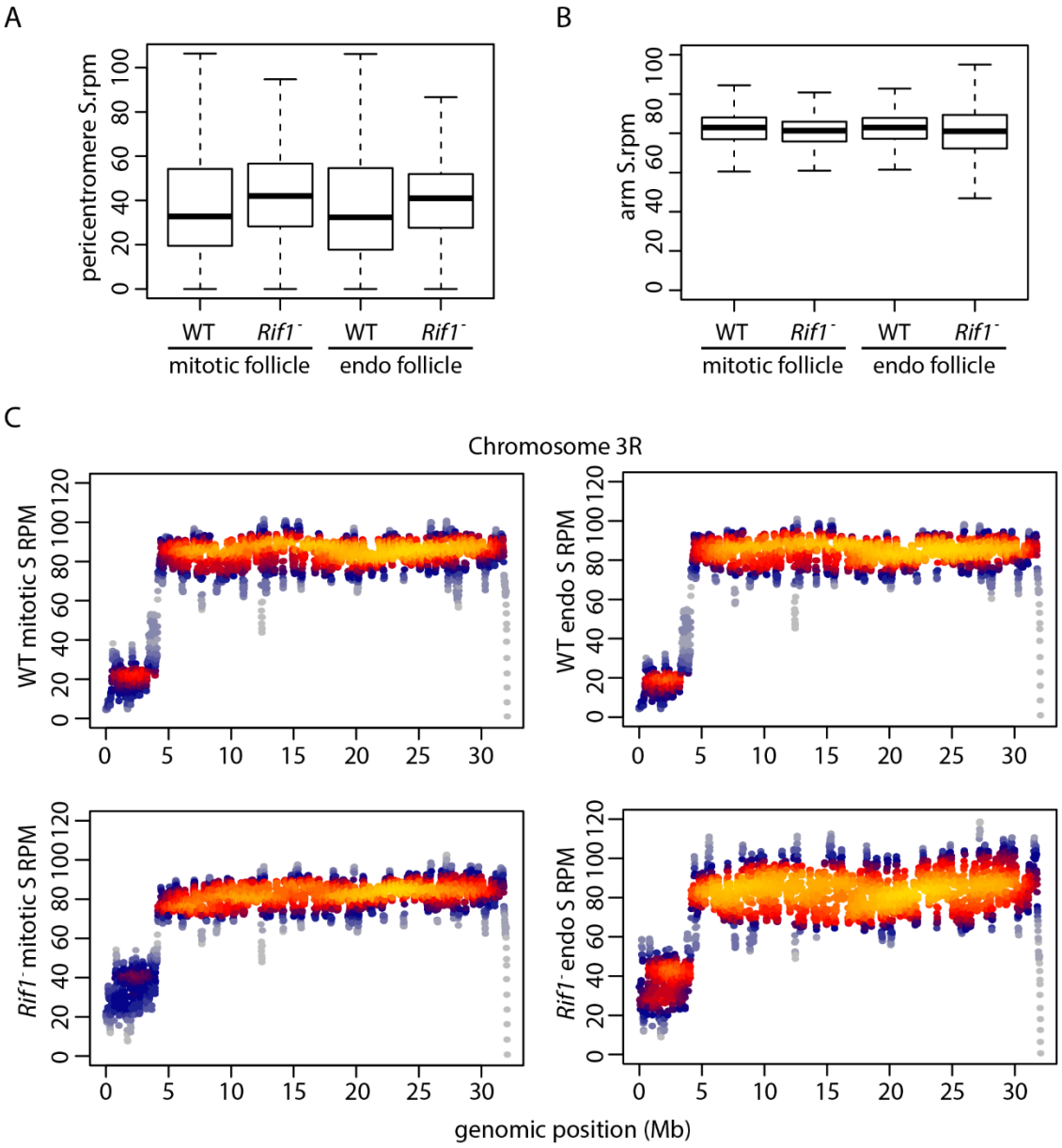

Figure S11. Under-replication does not contribute to RT differences between mitotically cycling and endocycling follicle cells. A-B) Boxplot of S phase copy number at pericentromeres (A) and chromosome arms (B) in wildtype (WT) and *Rif1*$^{-}$ mitotically cycling and endocycling follicle cells across all major chromosome scaffolds. **C)** Heatscatter plots of S phase copy number at 100kb windows with a 10kb slide across the Chromosome 3R scaffold in wildtype (WT) and *Rif1*$^{-}$ mitotically cycling (left) and endocycling (right) follicle cells.

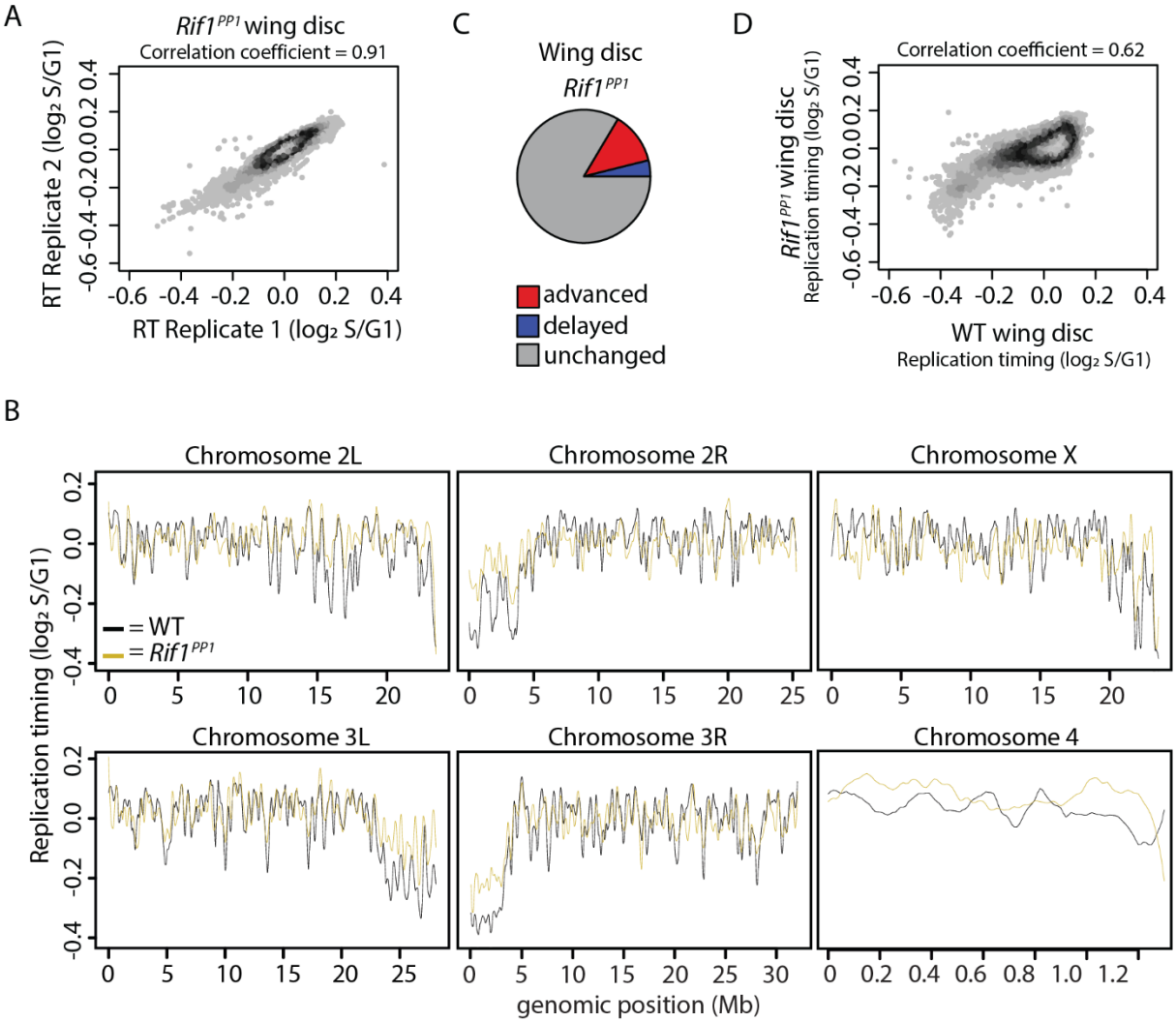

Figure S12. Characterization of RT in *Rif1*^{PP1} wing discs. A) Heatscatter plot comparing *Rif1*^{PP1} wing disc S/G1 (log_2) replicate replication timing values. **B)** LOESS regression line showing average S/G1 (log_2) replication timing values for wildtype wing discs (black) and *Rif1*^{PP1} wing discs (gold) at 100kb windows using a 10kb slide across the major chromosome scaffolds. **C)** Pie chart of all 100kb windows of significantly advanced (red), delayed (blue), and unchanged RT (grey) in *Rif1*^{PP1} wing discs across the major chromosome scaffolds. **D)** Heatscatter plot comparing wild type and *Rif1*^{PP1} wing disc S/G1 (log_2) ratios at 100kb windows using a 10kb slide across all major chromosome scaffolds.

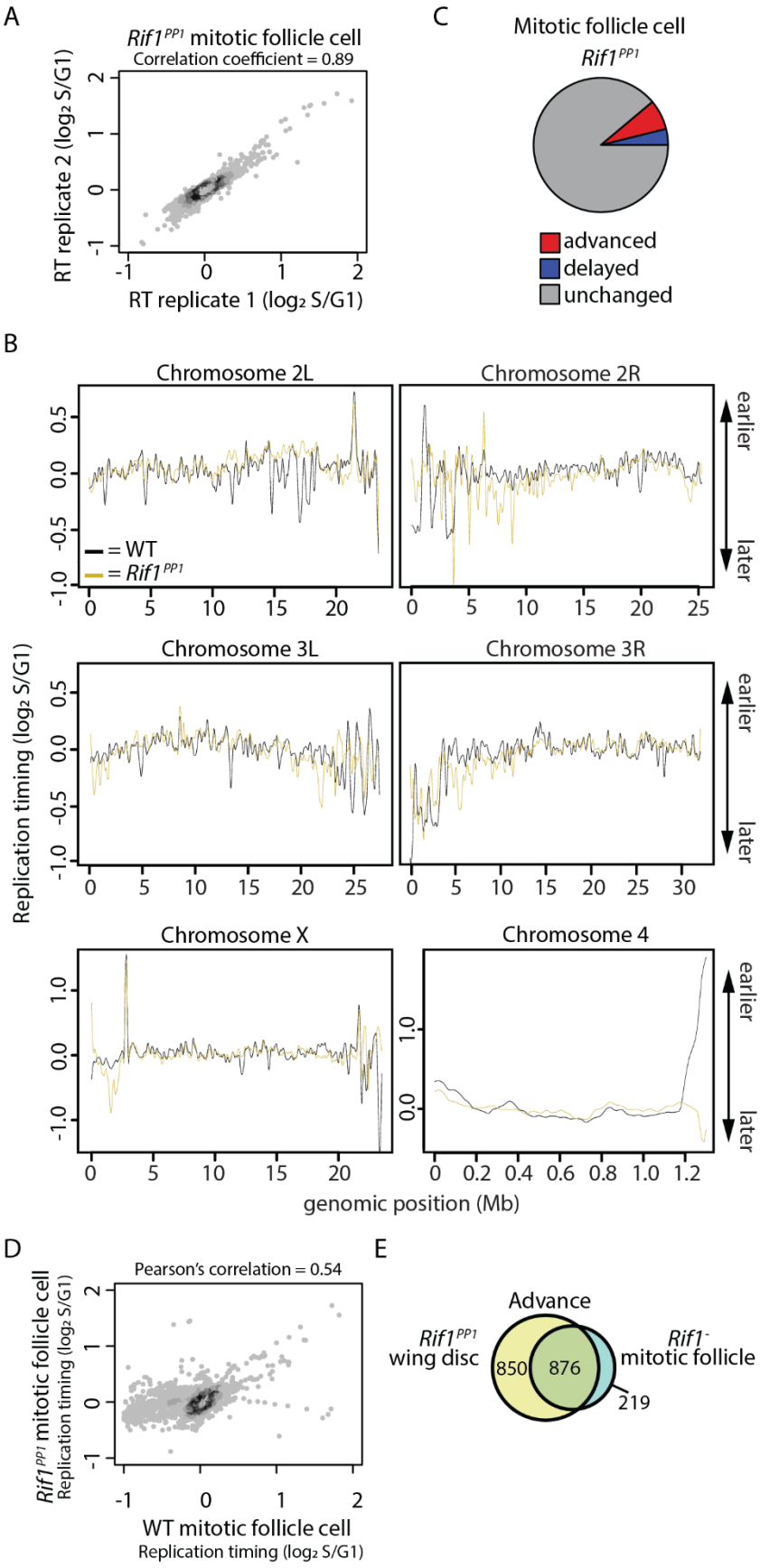
A
Rif1PP1 mitotic follicle cell
Correlation coefficient = 0.89
RT replicate 2 (log2 S/G1)
RT replicate 1 (log2 S/G1)
C
Mitotic follicle cell
Rif1PP1
advanced
delayed
unchanged
B
Chromosome 2L
Chromosome 2R
Chromosome 3L
Chromosome 3R
Chromosome X
Chromosome 4
= WT
= Rif1PP1
earlier
later
Replication timing (log2 S/G1)
genomic position (Mb)
D
Pearson's correlation = 0.54
Rif1PP1 mitotic follicle cell
Replication timing (log2 S/G1)
WT mitotic follicle cell
Replication timing (log2 S/G1)
E
Advance
Rif1PP1
wing disc
850
876
219
Rif1-
mitotic follicle

Figure S13. Characterization of RT in *Rif1^{PP1}* mitotic follicle cells. **A)** Heatscatter plot comparing *Rif1^{PP1}* mitotic follicle cell S/G1 (log_2) replicate replication timing values. **B)** LOESS regression line showing average S/G1 (log_2) replication timing values for wildtype mitotic follicle cells (black) and *Rif1^{PP1}* mitotic follicle cells (gold) at 100kb windows using a 10kb slide across the major chromosome scaffolds. **C)** Pie chart of all 100kb windows of significantly advanced (red), delayed (blue), and unchanged RT (grey) in *Rif1^{PP1}* mitotic follicle cells across the major chromosome scaffolds. **D)** Heatscatter plot comparing wild type and *Rif1^{PP1}* mitotic follicle cell S/G1 (log_2) ratios at 100kb windows using a 10kb slide across all major chromosome scaffolds. **E)** Venn diagram comparing advanced 100kb windows between *Rif1^{PP1}* wing discs (gold) and *Rif1^{-}* mitotic follicle cells (cyan).

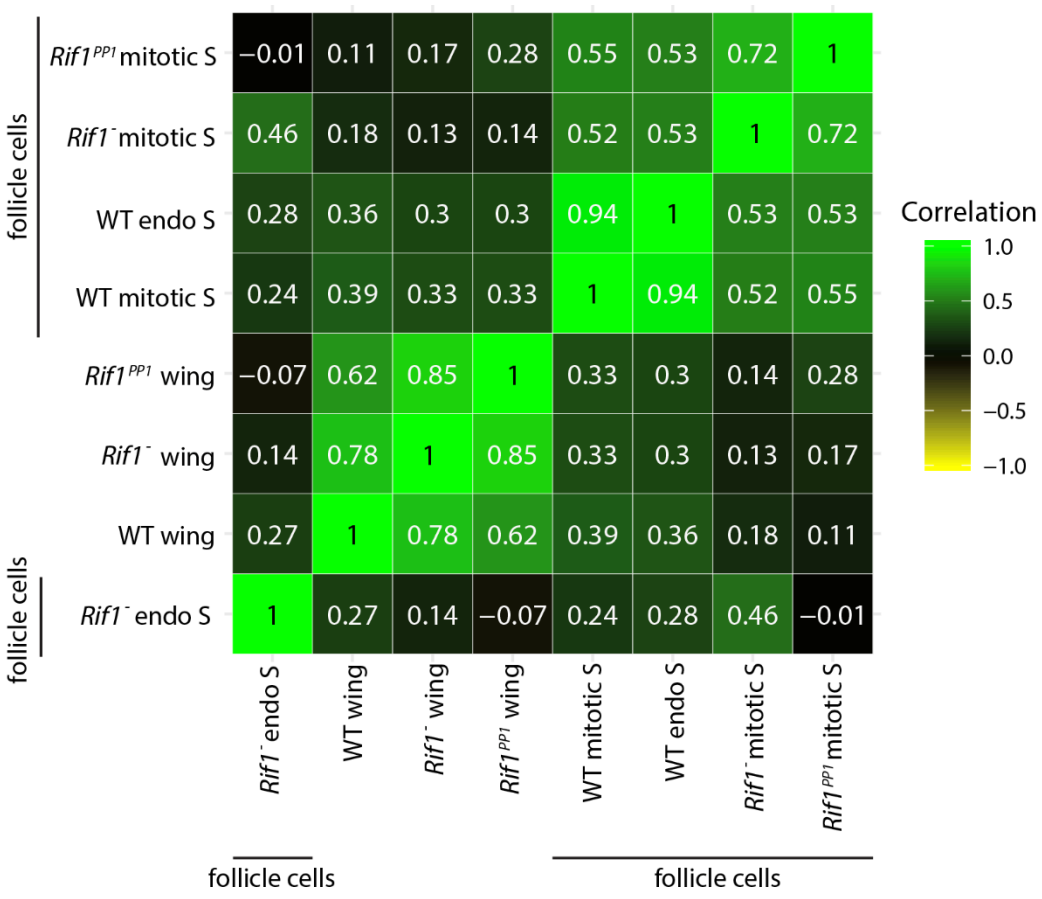

Figure S14. Correlation matrix of all replication timing datasets. Correlation matrix of S/G1 (log_2) replication timing values for wildtype mitotically cycling follicle cells (WT mitotic S), *Rif1*$^{-}$ mitotically cycling follicle cells (*Rif1*$^{-}$ mitotic S), *Rif1*^{PP1} mitotically cycling follicle cells (*Rif1*^{PP1} mitotic S), wildtype endocycling follicle cells (WT endo S), *Rif1*$^{-}$ endocycling follicle cells (*Rif1*$^{-}$ endo S), wild type wing discs (WT wing), *Rif1*$^{-}$ wing discs (*Rif1*$^{-}$ wing), and *Rif1*^{PP1} wing discs (*Rif1*^{PP1} wing). Correlation coefficients are indicated for each comparison.